ACS Macro Letters

Letter

pubs.acs.org/macroletters

Selective Nucleation of Poly(3-hexyl thiophene) Nanofibers on Multilayer Graphene Substrates

Daniel E. Acevedo-Cartagena,[†] Jiaxin Zhu,[‡] Elvira Trabanino,[§] Emily Pentzer,[†,∥] Todd Emrick,[†] Stephen S. Nonnenmann,[‡] Alejandro L. Briseno,*[,†] and Ryan C. Hayward*[,†]

[†]Department of Polymer Science and Engineering, University of Massachusetts—Amherst, Amherst, Massachusetts 01003, United States

[‡]Department of Mechanical and Industrial Engineering, University of Massachusetts—Amherst, Amherst, Massachusetts 01003, United States

[§]Department of Chemical Engineering, California State Polytechnic University—Pomona, Pomona, California 91768, United States

[∥]Department of Chemistry, Case Western Reserve University, Cleveland, Ohio 44106, United States

Supporting Information

ABSTRACT: We demonstrate that graphene surfaces provide highly selective nucleation of poly(3-hexyl thiophene) (P3HT) nanofibers (NFs) from supersaturated solutions. Solvent conditions are identified that give rise to a wide hysteresis between crystallization and melting centered around room temperature, yielding metastable solutions that are stable against homogeneous nucleation for long periods of time but that allow for heterogeneous nucleation by graphene. Selective growth of P3HT crystals is found for multilayer graphene (MLG) supported on either Si or ITO substrates, with nucleation kinetics that are more rapid for MLG on Si but slower in both cases than for highly oriented pyrolytic graphite (HOPG). Although the NFs grow vertically from the substrate with face-on orientation of P3HT chains, we observe edge-on orientation in dried films, presumably due to capillary forces that cause collapse of the NFs onto the substrate during solvent evaporation.

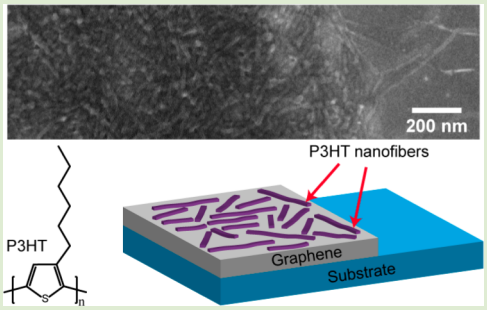

Solution-based assembly of conjugated organic materials represents a simple and scalable route to tailored crystalline nanostructures, offering potential pathways to low cost electronic devices with improved performance.[1] While conventional techniques to enhance crystallinity within device active layers (e.g., vapor or thermal annealing) often lead to structural coarsening, solution-based self-assembly can deliver highly crystalline structures with controlled nanoscale morphologies.[2] In the case of polymer-based heterojunction photovoltaic cells, which benefit from interpenetrating arrangements of crystalline domains of two materials,[2,3] one-dimensional (1D) crystalline nanostructures assembled in solution have been used to enhance device performance.[4,5] Moreover, attaining the proper orientation of conjugated molecules within active layers can enhance charge mobility along the relevant direction (i.e., toward the electrodes), offering further improvements in performance.[6−9] For conjugated polymers, high charge mobility is realized along the polymer chain backbone as well as through overlapping π orbitals between adjacent chains.[7] Therefore, an "edge-on" orientation (with the π planes of the polymer oriented perpendicular to the substrate) is beneficial for field effect transistors, which require high in-plane mobility values,[6] while "face-on" orientation (backbone π planes parallel to the substrate) is sought to increase out-of-plane charge transport in photovoltaic devices.[8]

Techniques for nanostructure assembly to provide the desired molecular ordering and orientation include the use of dip coating,[10] substrate rubbing,[11] zone casting,[12] and substrate-directed epitaxial growth.[13,14] Regioregular poly(3-hexyl thiophene) (P3HT) is among the most extensively studied conjugated polymers, selected for its high mobility (0.1 $cm^2 V^{-1} s^{-1}$), ease of synthesis, and tendency to assemble into crystalline nanofibers (NFs) suitable for electronic devices.[4,15,16] Graphene[17] and carbon nanotubes[18] represent attractive platforms for directing organization of P3HT into 1D nanostructures, where $\pi-\pi$ and van der Waals interactions drive face-on adsorption of P3HT chains.[8,19] Moreover, graphene offers a potential alternative to indium tin oxide (ITO) as a transparent conductive electrode for photovoltaic devices,[20] therefore suggesting the possibility to directly nucleate and orient conjugated polymer nanostructures within the active layers of graphene-based devices. However, while suspensions of reduced graphene oxide have been shown to nucleate P3HT NFs from solution[17] and graphene is known to modify orientation of crystals in thin P3HT films,[8,19] the use of

Received: January 19, 2015
Accepted: April 8, 2015
Published: April 14, 2015

ACS Publications © 2015 American Chemical Society

DOI: 10.1021/acsmacrolett.5b00038
ACS Macro Lett. 2015, 4, 483−487

a graphene electrode surface to direct growth of conjugated polymer nanostructures from solution has not been reported.

Here, we present a simple method for selective growth of P3HT NFs directly onto multilayer graphene (MLG) coated Si and ITO substrates, as well as on highly oriented pyrolytic graphite (HOPG). To achieve selective crystallization on these nucleating surfaces, a metastable P3HT solution is needed for which the level of supersaturation is sufficient to allow heterogeneous nucleation but insufficient to induce homogeneous nucleation. As a solvent, we choose *m*-xylene, which was found by Oh et al.[21] to provide a high degree of crystallinity and a wide hysteresis window between crystallization and melting temperatures for P3HT NFs. We use a relatively low molecular weight P3HT (polystyrene equivalent M_n = 12 kg/mol and $Đ$ = 1.28 by GPC; regioregularity = 93% by ^{1}H NMR) at a concentration of 0.50 mg/mL; as shown below, a wide hysteresis window centered around room temperature is observed, thereby facilitating NF growth experiments. Generalizing to higher molecular weight samples would likely require the use of a slightly better solvent for P3HT or an elevated growth temperature.

The degree of P3HT aggregation is assessed using UV−vis spectroscopy, as summarized in Figure 1. As described in the Supporting Information, we use a method based on filtration of NF suspensions crystallized to different extents to estimate the absorption coefficient $\varepsilon_f = 20 \pm 2$ mL cm^{-1} mg^{-1} for absorption by the NFs at 602 nm (A_{602}), the vibronic peak corresponding to the 0−0 transition in the aggregated state.[22] From the UV−vis spectrum of a given sample with known total P3HT concentration c, a direct measurement of the aggregated fraction x_f can be calculated from the Beer−Lambert law, i.e., $x_f = A_{602}/(\varepsilon_f c l)$, where l is the path length for the UV−vis measurement. We note that the value of x_f is likely larger than the crystalline fraction x_c since the NFs presumably possess amorphous regions,[23] but it nonetheless provides a useful proxy for the degree of crystallization.

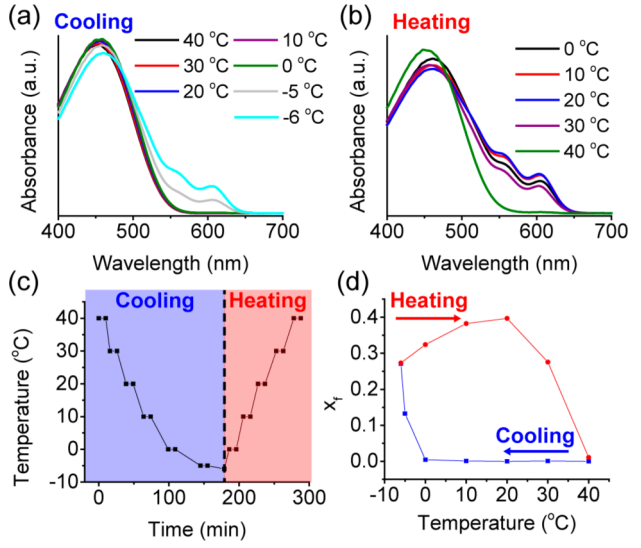

Figure 1. UV−vis spectra of a 0.50 mg/mL solution of P3HT in *m*-xylene during (a) cooling and (b) heating, along with (c) the temperature profile employed (the sample was held for at least 10 min at each temperature) and (d) the degree of aggregation x_f measured during the temperature cycle.

The hysteresis between crystallization and melting of P3HT NFs with changes in temperature is clearly seen in Figure 1d. No aggregation is observed at room temperature on a time scale of ∼10 min, but upon cooling below 0 °C, P3HT rapidly crystallizes into NFs that remain stable until they are heated to 40 °C. Interestingly, x_f increases while heating from −5 to 20 °C, a result of slow crystallization kinetics compared to the rate of heating and melting of some fraction of the crystals formed at low temperature as they warm to room temperature during the UV−vis measurement (see Figure S5, Supporting Information). Regardless, data in Figure 1d clearly demonstrate that at room temperature a sizable thermodynamic driving force for crystallization exists, while the rate of crystal nucleation in solution is low.

Remarkably, incubation of ITO substrates partially coated with MLG in the metastable solution at room temperature leads to highly selective crystallization of P3HT, as evidenced by the MLG-coated area developing a purple color while the uncoated portion remains colorless (Figure 2a). The absorbance spectra of these deposited films show vibronic peaks characteristic of crystalline P3HT, which increase in intensity monotonically with time due to the growth of NFs. Similarly, atomic force microscopy (AFM) and optical profilometry measurements reveal a slow increase in the average film thickness with time, up to 5.4 ± 0.8 nm after 120 h of incubation. Assuming a density of 1.1 g/mL for P3HT,[24] these thicknesses can be compared to the UV−vis spectra (Figure S3a, Supporting Information) to determine an absorption coefficient at 602 nm for the solid films (ε_s). Interestingly, the value of $\varepsilon_s = 270 \pm 30$ mL cm^{-1} mg^{-1} is more than an order of magnitude larger than the value of ε_f for the suspended NFs. Since the electric transition dipole of P3HT is oriented along the chain axis,[25] orientation of NFs within the solid film should lead to a 3-fold increase in absorption of light with normal incidence, compared to a randomly oriented suspension.[26] Additionally, the dried film shows a more intense absorption for the 0−0 transition relative to the 0−1 and 0−2 peaks (Figure S3, Supporting Information), corresponding to increased intrachain planarity (*J*-aggregate character) in the dried NFs compared to those in suspension.[22]

Surprisingly, as seen in Figure 2b, the rate of crystallization is substantially faster when a silicon wafer is used as the underlying substrate instead of ITO, leading to an average film thickness of 20 nm within 24 h, followed by slower growth. Examination of the interface between the graphene-coated regions and the bare substrates with scanning electron microscopy (SEM, Figure 2c,d) reveals that the P3HT films are composed of NFs with lengths over 100 nm in both cases. For MLG on Si, the surface is completely covered by NFs. For MLG on ITO, the density of nanowires is lower, and some portions of the graphene surface remain exposed. These observations are consistent with the measured average film thicknesses of 1.2 ± 0.6 nm for MLG on ITO and 20 ± 1 nm for MLG on Si following 24 h of growth since the individual NFs are 3 ± 1 nm thick. P3HT crystallization remains highly selective to MLG on both substrates; while NFs that presumably nucleated on the graphene surface stretch several hundred nanometers away from the interface onto the bare substrate surface (Figure S10, Supporting Information), no NFs are observed further from the interface. Furthermore, the occurrence of NFs on MLG clearly results from surface-driven nucleation rather than adsorption of solution-nucleated structures since the metastable solutions show no evidence of

DOI: 10.1021/acsmacrolett.5b00038
ACS Macro Lett. 2015, 4, 483−487

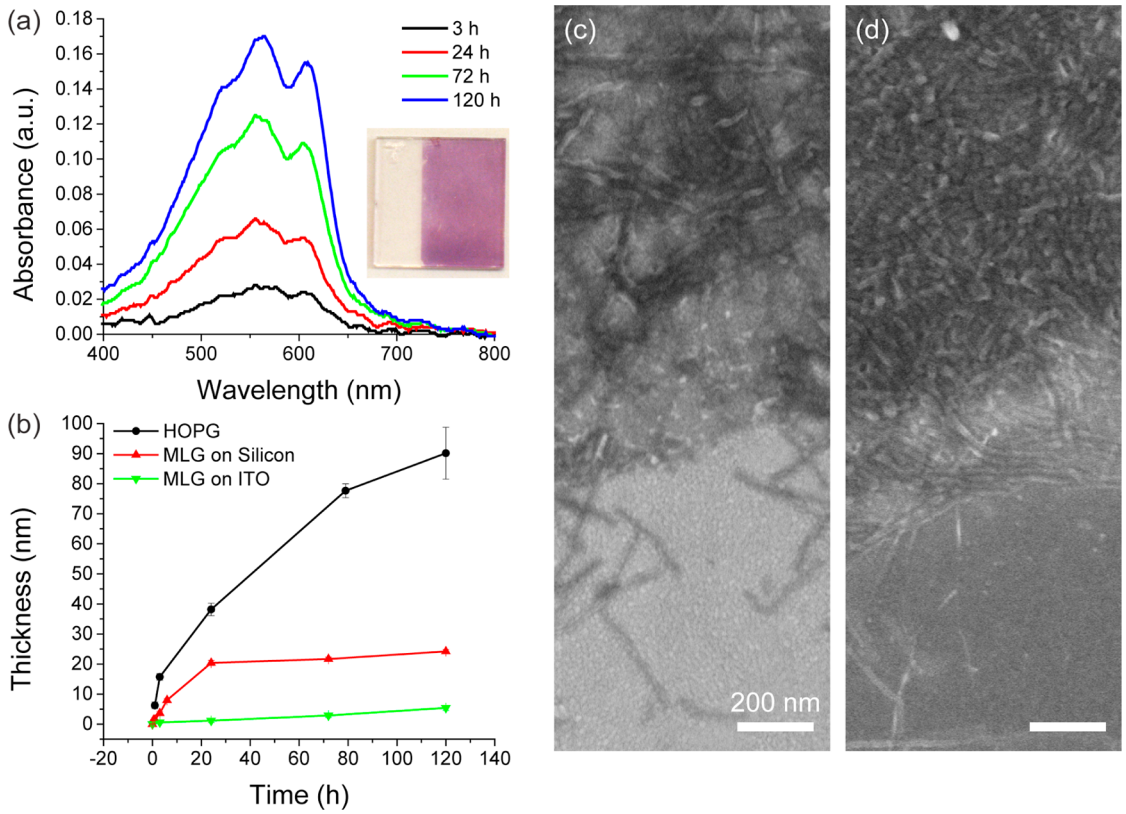

Figure 2. (a) UV−vis absorbance spectra of P3HT films grown on MLG on ITO at different times of incubation in a metastable solution of P3HT. The inset shows a photograph of a film of P3HT formed for 120 h on ITO coated with MLG only on the right side. (b) Thicknesses of P3HT films as a function of incubation time determined by AFM for MLG on Si (red) and HOPG (black) and by optical profilometry for MLG on ITO (green). Error bars represent one standard deviation based on 10 measurements. SEM images of the interface between MLG-coated regions (top) and the bare substrate (bottom) after 24 h of growth using (c) ITO and (d) Si substrates.

NF formation by UV−vis even after 120 h of aging at room temperature (Figure S4, Supporting Information).

The observed sensitivity of crystallization kinetics to the underlying substrate may arise from a number of factors. van der Waals interactions with the substrate likely represent an important contribution and should be stronger for Si (covered with a thin layer of native oxide) than for ITO: respective estimated polarizability values for Si and ITO are 3.8 and 0.6 Å^3 based on the Clausius−Mossotti relation and literature dielectric constants;[27,28] the polarizability of SiO_2 (2.5 Å^3 as determined in a previous study[29]) is smaller than that of Si but still larger than ITO. The higher polarizability of HOPG compared to MLG (also invoked by Shokri et al.[30] to explain stronger adsorption of substituted aromatic molecules on HOPG) may be responsible for the high rates of growth on HOPG, although making a direct comparison is complicated by the relatively high defect density of MLG grown by chemical vapor deposition, as employed here. Substrate roughness may also play a role: as seen in Figure 2c, ITO is composed of grains with average sizes of 15 nm, which is comparable to the contour length of the P3HT chains,[31] possibly impeding crystal nucleation compared to the smoother Si surface. In addition, since the interaction between P3HT and graphene involves a degree of charge transfer,[32] the impact of the underlying substrate on the electronic state of graphene could influence the nucleation rates. As seen in Figure 2b, the film thickness of P3HT NFs grown on MLG on Si and on HOPG saturates, or at least slows considerably, in the later stages of growth. Since the solutions are agitated throughout growth, this should not be due to diffusion limitations. Instead, we suspect that this behavior reflects self-poisoning of NFs caused by the accumulation of defects or by the competition between crystallization of folded and extended chains[33] since the molecular weight of P3HT used (M_n = 12 kg/mol) is just above the threshold for chain folding (10 kg/mol).[34]

Additional insight into how graphene and HOPG substrates direct P3HT NF growth is provided by SEM images showing the evolution of film morphology with time. During the initial stages of growth on HOPG and MLG on Si (Figure 3a,c), individual NFs with lengths below 50 nm and widths of 16 ± 2 nm are observed. For MLG on Si, the short NFs in Figure 3c are observed after approximately 0.5 h, while for HOPG a high density of short NFs are seen at 5 min (Figure 3a). At 3 h (Figure 3b,d) HOPG is completely covered with NFs, and MLG on Si shows long NFs. However, for MLG on ITO (Figure 3e,f), no evidence of NFs is seen at 3 h, while after 24 h, long NFs are observed. These results are consistent with a similar rate of growth of NFs on each substrate but a nucleation rate that increases from MLG on ITO, to MLG on Si, to HOPG.

Since P3HT chains have been reported to adsorb with face-on orientation on MLG[19] and HOPG,[35] and the direction of π-stacking is along the long axis of the fibers, we expect that NFs initially grow perpendicular to the substrate. However, the NFs observed by SEM in the dried films orient parallel to the substrate, even at the longest time studied (120 h), as seen in Figure 4. Moreover, grazing incidence wide-angle X-ray scattering (GIWAXS) measurements reveal strong (h00)

DOI: 10.1021/acsmacrolett.5b00038
ACS Macro Lett. 2015, 4, 483−487

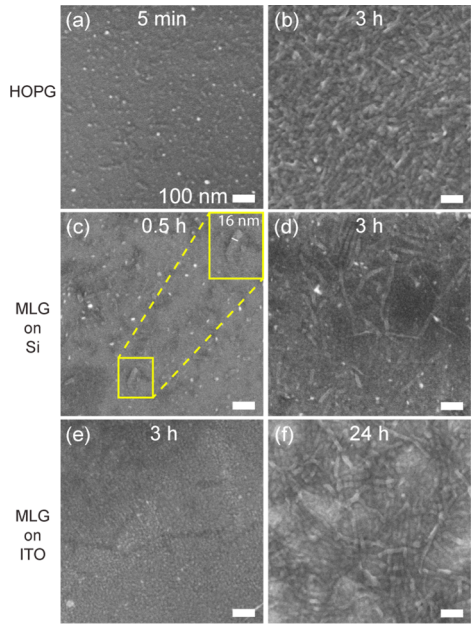

Figure 3. SEM images of P3HT grown from a metastable solution on different substrates: HOPG for (a) 5 min and (b) 3 h; MLG on Si for (c) 0.5 h and (d) 3 h; and MLG on ITO for periods of (e) 3 h and (f) 24 h. The inset in (c) shows an individual short NF.

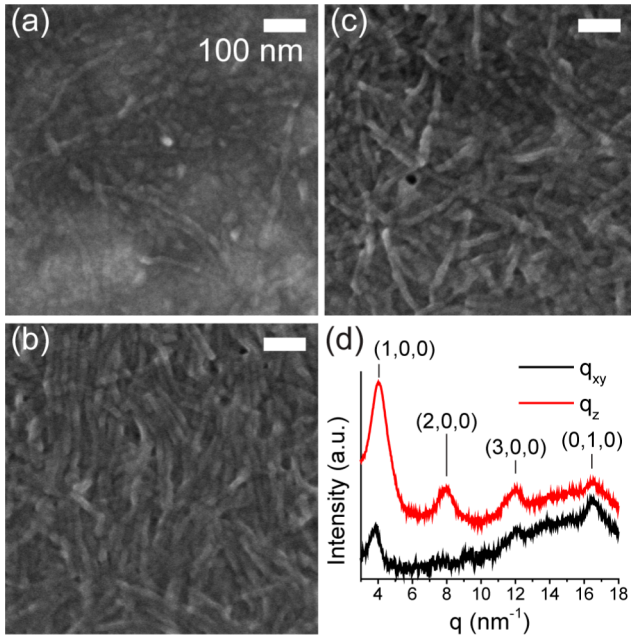

Figure 4. SEM images of P3HT NFs grown from a metastable solution for 120 h on (a) MLG on ITO, (b) MLG on Si, and (c) HOPG. (d) Grazing incidence wide-angle X-ray scattering from P3HT films grown for 120 h on MLG on Si.

reflections and no clear (010) reflection along the out-of-plane direction q_z, with much weaker (h00) reflections and a clear (010) peak along the in-plane direction q_{xy}, further confirming the edge-on orientation of crystalline NFs in the dried films (Figure 4d and Figure S11, Supporting Information).

To establish that NFs are nucleated by the substrate with a face-on orientation, we perform *in situ* atomic force microscopy (AFM) measurements during fiber growth on HOPG from metastable solutions (Figure 5a). After 3 h of growth,

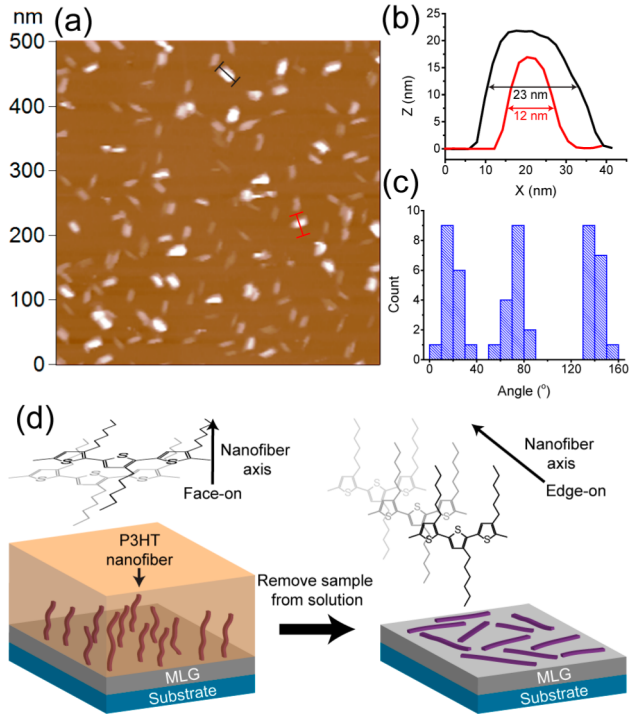

Figure 5. (a) *In situ* AFM image of NFs growing from HOPG at 3 h of incubation in a metastable solution. (b) Cross-sectional profiles across the long (black) and short (red) axes of the NFs as indicated in (a), with their respective full widths at half-maximum indicated. (c) Distribution of the orientation of the long axis of NFs relative to the horizontal direction in (a). (d) A schematic illustration of NFs grown in solution before (left) and after (right) removing the substrate from the fluid, with their respective chain orientations.

anisotropic NFs with in-plane dimensions of ≈20 nm × 10 nm are observed, consistent with the widths (16 ± 2 nm) and thicknesses (3 ± 1 nm) of NFs, respectively, after taking into account the convolution between the NFs and the AFM tip size (radius 9 ± 2 nm). The out-of-plane dimensions range up to ~20 nm (Figure 5c)—much larger than the thickness expected for a NF with side-on orientation (3 nm)—and can be seen to increase over time, indicating that growth occurs along the vertical direction. These observations establish that nucleation occurs on the surface of HOPG with a face-on orientation, followed by growth into vertically oriented NFs. Moreover, the long axes of NFs (i.e., the direction of the polymer backbone) show three preferred orientations each differing by ~60° (Figure 5c). This is consistent with epitaxial nucleation, as expected based on previous *in situ* measurements showing face-on epitaxial adsorption of P3HT on HOPG.[35]

Since NFs grow from the substrate in a face-on orientation, the edge-on structure in dried films can therefore be attributed to capillary collapse during solvent removal, as illustrated in Figure 5d. For a ribbon with thickness t, width w, and bending stiffness, $B = (\bar{E}t^3w)/12$, surface tension γ will cause buckling beyond a critical length[36]

$$l_c = \sqrt{\frac{B\pi^2}{8\gamma(t+w)}}$$

Using measured values of t = 3 nm and w = 16 nm, along with the surface tension γ = 0.029 N/m for m-xylene and a plane-strain modulus for P3HT of $\bar{E}$ = 1.2 GPa,[37] we estimate a value of l_c = 10 nm. Thus, the flexibility of the thin NFs means that

DOI: 10.1021/acsmacrolett.5b00038
ACS Macro Lett. 2015, 4, 483−487

surface tension is sufficient to cause collapse of NFs oriented vertically in solution into a consolidated film with predominantly in-plane orientation.

In conclusion, we have demonstrated a method for selective solution crystallization of P3HT NFs from graphene surfaces. Surprisingly, the rate of crystal nucleation is found to be highly dependent on the underlying substrate, suggesting a potential route for further tailoring crystallization kinetics. Although NFs grow vertically due to face-on adsorption of P3HT chains, capillary forces can cause collapse into a horizontally oriented film upon solvent evaporation. Given that other conjugated organic materials undergo epitaxial absorption and nucleation on graphene[14,38] and carbon nanotubes,[18] it will be interesting to explore whether the method developed here can be extended to other conjugated polymers.

■ ASSOCIATED CONTENT

Supporting Information

Experimental procedures, optical profilometry and AFM measurements, calibration plots to determine the absorption coefficient of P3HT, and control experiments. This material is available free of charge via the Internet at http://pubs.acs.org.

■ AUTHOR INFORMATION

Corresponding Authors

*E-mail: hayward@umass.edu

*E-mail: abriseno@mail.pse.umass.edu

Notes

The authors declare no competing financial interest.

■ ACKNOWLEDGMENTS

The work was primarily supported by the Department of Energy (Grant DE-SC0006639; solution state measurements, characterization of growth kinetics and film morphology), with additional support from the Office of Naval Research (Award N00014710410053; graphene substrate preparation) and the National Science Foundation (CHE-1152360; synthesis of P3HT). Partial fellowship support for D.A.-C. was provided by the NSF through the Graduate Research Fellowship Program (Grant 2013162353) and the Northeast Alliance for Graduate Education and the Professoriate (HRD-0450339), along with REU support for E.T. from the NSF MRSEC on Polymers at UMass (DMR-0820506). The GIWAXS measurements were carried out at the Stanford Synchrotron Radiation Light Source. The authors thank Yue Zhang for assistance with graphene substrate preparation.

■ REFERENCES

(1) Diao, Y.; Shaw, L.; Bao, Z.; Mannsfeld, S. C. B. *Energy Environ. Sci.* **2014**, *7*, 2145−2159.

(2) Nagarjuna, G.; Venkataraman, D. *J. Polym. Sci., Part B: Polym. Phys.* **2012**, *50*, 1045−1056.

(3) Wang, M.; Wudl, F. *J. Mater. Chem.* **2012**, *22*, 24297−24314.

(4) Ren, G.; Ahmed, E.; Jenekhe, S. A. *J. Mater. Chem.* **2012**, *22*, 24373−24379.

(5) Briseno, A. L.; Mannsfeld, S. C. B.; Jenekhe, S. A.; Bao, Z.; Xia, Y. *Mater. Today* **2008**, *11*, 38−47.

(6) Sirringhaus, H.; Brown, P. J.; Friend, R. H.; Nielsen, M. M.; Bechgaard, K.; Langeveld-Voss, B. M. W.; Spiering, A. J. H.; Janssen, R. A. J.; Meijer, E. W.; Herwig, P.; de Leeuw, D. M. *Nature* **1999**, *401*, 685−688.

(7) Yao, Y.; Dong, H.; Hu, W. *Polym. Chem.* **2013**, *4*, 5197−5205.

(8) Skrypnychuk, V.; Boulanger, N.; Yu, V.; Hilke, M.; Mannsfeld, S. C. B.; Toney, M. F.; Barbero, D. R. *Adv. Funct. Mater.* **2014**, 664−670.

(9) Zhang, Y.; Diao, Y.; Lee, H.; Mirabito, T. J.; Johnson, R. W.; Puodziukynaite, E.; John, J.; Carter, K. R.; Emrick, T.; Mannsfeld, S. C. B.; Briseno, A. L. *Nano Lett.* **2014**, *14*, 5547−5554.

(10) Wang, S.; Kiersnowski, A.; Pisula, W.; Müllen, K. *J. Am. Chem. Soc.* **2012**, *134*, 4015−4018.

(11) Lee, M. J.; Gupta, D.; Zhao, N.; Heeney, M.; McCulloch, I.; Sirringhaus, H. *Adv. Funct. Mater.* **2011**, *21*, 932−940.

(12) Biniek, L.; Pouget, S.; Djurado, D.; Gonthier, E.; Tremel, K.; Kayunkid, N.; Zaborova, E.; Crespo-Monteiro, N.; Boyron, O.; Leclerc, N.; Ludwigs, S.; Brinkmann, M. *Macromolecules* **2014**, *47*, 3871−3879.

(13) Hartmann, L.; Tremel, K.; Uttiya, S.; Crossland, E.; Ludwigs, S.; Kayunkid, N.; Vergnat, C.; Brinkmann, M. *Adv. Funct. Mater.* **2011**, *21*, 4047−4057.

(14) Wise, A. J.; Zhang, Y.; Fan, J.; Wudl, F.; Briseno, A. L.; Barnes, M. D. *Phys. Chem. Chem. Phys.* **2014**, *16*, 15825−15830.

(15) Kim, J. S.; Lee, J. H.; Park, J. H.; Shim, C.; Sim, M.; Cho, K. *Adv. Funct. Mater.* **2011**, *21*, 480−486.

(16) Oosterbaan, W. D.; Vrindts, V.; Berson, S.; Guillerez, S.; Douhéret, O.; Ruttens, B.; D'Haen, J.; Adriaensens, P.; Manca, J.; Lutsen, L.; Vanderzande, D. *J. Mater. Chem.* **2009**, *19*, 5424−5435.

(17) Chunder, A.; Liu, J.; Zhai, L. *Macromol. Rapid Commun.* **2010**, *31*, 380−384.

(18) Liu, J.; Moo-Young, J.; McInnis, M.; Pasquinelli, M. A.; Zhai, L. *Macromolecules* **2014**, *47*, 705−712.

(19) Kim, D. H.; Lee, H. S.; Shin, H.-J.; Bae, Y.-S.; Lee, K.-H.; Kim, S.-W.; Choi, D.; Choi, J.-Y. *Soft Matter* **2013**, *9*, 5355−5360.

(20) Gomez De Arco, L.; Zhang, Y.; Schlenker, C. W.; Ryu, K.; Thompson, M. E.; Zhou, C. *ACS Nano* **2010**, *4*, 2865−2873.

(21) Oh, J. Y.; Shin, M.; Lee, T., Il; Jang, W. S.; Min, Y.; Myoung, J.-M.; Baik, H. K.; Jeong, U. *Macromolecules* **2012**, *45*, 7504−7513.

(22) Niles, E. T.; Roehling, J. D.; Yamagata, H.; Wise, A. J.; Spano, F. C.; Moulé, A. J.; Grey, J. K. *J. Phys. Chem. Lett.* **2012**, *3*, 259−263.

(23) Nieuwendaal, R. C.; Snyder, C. R.; DeLongchamp, D. M. *ACS Macro Lett.* **2014**, *3*, 130−135.

(24) Koch, F. P. V.; Heeney, M.; Smith, P. *J. Am. Chem. Soc.* **2013**, *135*, 13699−13709.

(25) Zhokhavets, U.; Gobsch, G.; Hoppe, H.; Sariciftci, N. S. *Thin Solid Films* **2004**, *451*−*452*, 69−73.

(26) Thulstrup, E. W.; Thulstrup, P. W. *Acta Chim. Slov.* **2005**, *52*, 371−383.

(27) *Handbook of Chemistry and Physics*, 95th ed.; Haynes, W. M., Thomas, B., Lide, D. R., Eds.; CRC Press: Boca Raton, FL, 2014; pp 47−55.

(28) Gerfin, T.; Grätzel, M. *J. Appl. Phys.* **1996**, *79*, 1722−1729.

(29) Bruch, L. *Phys. Rev. B* **2005**, *72*, 033410.

(30) Shokri, R.; Vonau, F.; Cranney, M.; Aubel, D.; Narladkar, A.; Isare, B.; Bouteiller, L.; Simon, L.; Reiter, G. *J. Phys. Chem. C* **2012**, *116*, 21594−21600.

(31) Holdcroft, S. *J. Polym. Sci., Part B: Polym. Phys.* **1991**, *29*, 1585−1588.

(32) Abd Wahab, F.; Sulaiman, K.; Huang, N. M. *J. Electron. Mater.* **2013**, *42*, 2739−2742.

(33) Ma, Y.; Qi, B.; Ren, Y.; Ungar, G.; Hobbs, J. K.; Hu, W. *J. Phys. Chem. B* **2009**, *113*, 13485−13490.

(34) Liu, J.; Arif, M.; Zou, J.; Khondaker, S. I.; Zhai, L. *Macromolecules* **2009**, *42*, 9390−9393.

(35) Mena-Osteritz, E.; Meyer, A.; Langeveld-Voss, B. M. W.; Janssen, R. A. J.; Meijer, E. W.; Bäuerle, P. *Angew. Chem., Int. Ed. Engl.* **2000**, *39*, 2679−2684.

(36) Roman, B.; Bico, J. *J. Phys.: Condens. Matter* **2010**, *22*, 493101−493116.

(37) Savagatrup, S.; Makaram, A. S.; Burke, D. J.; Lipomi, D. J. *Adv. Funct. Mater.* **2014**, *24*, 1169−1181.

(38) Majumdar, D.; Baskey, M.; Saha, S. K. *Macromol. Rapid Commun.* **2011**, *32*, 1277−1283.

DOI: 10.1021/acsmacrolett.5b00038
ACS Macro Lett. 2015, 4, 483−487